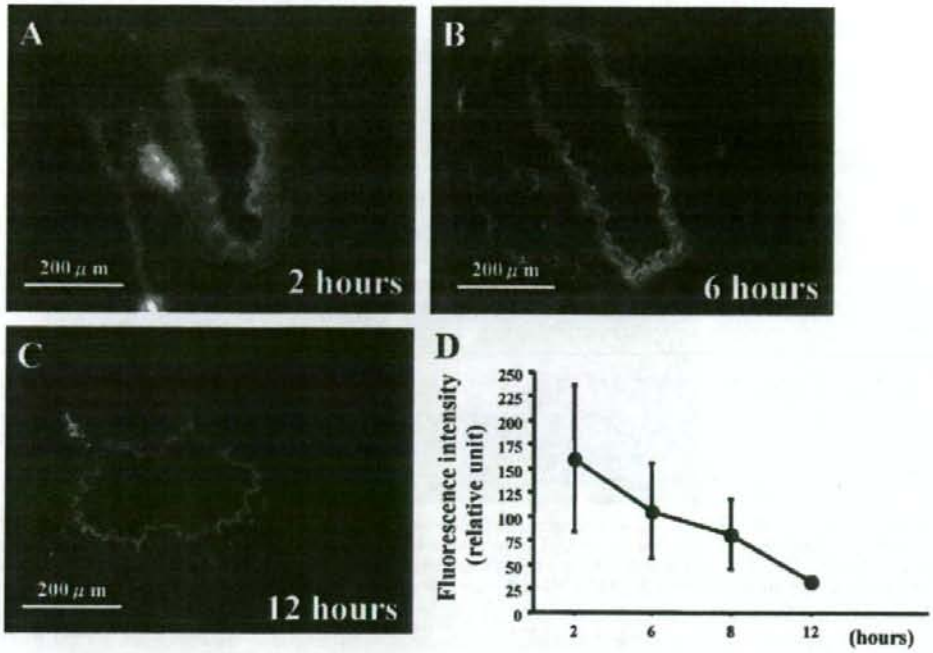

Figure 6. A through D, Time-dependent changes of the level of transduced 11R-EGFP in BAs after SAH induction. The protein level of 11R-EGFP reached maximum 2 hours after injection (A). However, the level gradually decreased over a 12-hour period (B and C). Signals were analyzed by Scion Image.

with only a single injection of the protein. These characteristics of the protein therapy may be suitable for acute but transient cerebrovascular disorders such as cerebral vasospasm after SAH or stroke rather than chronic medical condition like the pathology of cancer. Interestingly, all kinds of proteins, peptides, and therapeutic drugs can be transduced into cells by protein therapy.[22,28,32] Therefore, we will have to examine whether 11R-fused vasoactive proteins such as endothelial nitric oxide synthase or calcitonin gene-related peptide were also efficiently delivered into cerebral arteries and have contractile or relaxant responses to cerebral arteries in the coming years. The 11R–endothelial nitric oxide synthase experiment for the treatment of cerebral vasospasm is now ongoing in our laboratory.

Conclusions

The 11R-EGFP was effectively, directly, and immediately delivered into the BA walls, especially into the smooth muscle layers, both ex vivo and in vivo. This is the first study to our knowledge to demonstrate the successful transduction of a PTD-fused protein into the cerebral arteries. We will have to examine whether PTD-fused vasoactive proteins are also effectively transduced into cerebral arteries and have a therapeutic effect on cerebrovascular diseases including cerebral vasospasm after SAH in the future.

Acknowledgments

The authors thank A. Kemori, M. Arao, and T. Ujibashi for technical assistance.

Sources of Funding

This work was supported in part by grants-in-aid for scientific research from the Ministry of Education, Culture, Sports, and Technology, Japan.

Disclosure

None.

References

1. Khurana VG, Smith LA, Baker TA, Eguchi D, O'Brien T, Katusic ZS. Protective vasomotor effects of in vivo recombinant endothelial nitric oxide synthase gene expression in a canine model of cerebral vasospasm. *Stroke*. 2002;33:782–789.
2. Muhonen MG, Ooboshi H, Welsh MJ, Davidson BL, Heistad DD. Gene transfer to cerebral blood vessels after subarachnoid hemorrhage. *Stroke*. 1997;28:822–828.
3. Toyoda K, Faraci FM, Russo AF, Davidson BL, Heistad DD. Gene transfer of calcitonin gene-related peptide to cerebral arteries. *Am J Physiol*. 2000;278:H586–H594.
4. Onoue H, Tsutsui M, Smith L, Stelter A, O'Brien T, Katusic ZS. Expression and function of recombinant endothelial nitric oxide synthase gene in canine basilar artery after experimental subarachnoid hemorrhage. *Stroke*. 1998;29:1959–1966.
5. McGirt MJ, Parra A, Sheng H, Higuchi Y, Oury TD, Laskowitz DT, Pearlstein RD, Warner DS. Attenuation of cerebral vasospasm after subarachnoid hemorrhage in mice overexpressing extracellular superoxide dismutase. *Stroke*. 2002;33:2317–2323.
6. Watanabe Y, Chu Y, Andresen JJ, Nakane H, Faraci FM, Heistad DD. Gene transfer of extracellular superoxide dismutase reduces cerebral vasospasm after subarachnoid hemorrhage. *Stroke*. 2003;34:434–440.
7. Ono S, Komuro T, Macdonald RL. Heme oxygenase-1 gene therapy for prevention of vasospasm in rats. *J Neurosurg*. 2002;96:1094–1102.
8. Satoh M, Perkins E, Kimura H, Tang J, Chun Y, Heistad DD, Zhang JH. Posttreatment with adenovirus-mediated gene transfer of calcitonin gene-

related peptide to reverse cerebral vasospasm in dogs. *J Neurosurg.* 2002;97:136–142.
9. Chen AFY, Jiang S-W, Crotty TB, Tsutsui M, Smith LA, O'Brien T, Katusic ZS. Effects of in vivo adventitial expression of recombinant endothelial nitric oxide synthase gene in cerebral arteries. *Proc Natl Acad Sci U S A.* 1997;94:12568–12573.
10. Verma IM, Somia N. Gene therapy—promises, problems and prospects. *Nature (Lond).* 1997;389:239–242.
11. Dorsch NW. Therapeutic approaches to vasospasm in subarachnoid hemorrhage. *Curr Opin Crit Care.* 2002;8:128–133.
12. Heistad DD, Faraci FM. Gene therapy for cerebral vascular disease. *Stroke.* 1996;27:1688–1693.
13. Templeton NS, Lasic DD, Frederik PM, Strey HH, Roberts DD, Pavlakis GN. Improved DNA: liposome complexes for increased systemic delivery and gene expression. *Nat Biotechnol.* 1997;15:647–652.
14. Templeton NS, Lasic DD. New directions in liposome gene delivery. *Mol Biotechnol.* 1999;11:175–180.
15. Ono S, Date I, Onoda K, Shiota T, Ohmoto T, Ninomiya Y, Asari S, Morishita R. Decoy administration of NF-kappaB into the subarachnoid space for cerebral angiopathy. *Hum Gene Ther.* 1998;9:1003–1011.
16. Jin LH, Bahn JH, Eum WS, Kwon HY, Jang SH, Han KH, Kang TC, Won MH, Kang JH, Cho SW, Park J, Choi SY. Transduction of human catalase mediated by an HIV-1 TAT protein basic domain and arginine-rich peptides into mammalian cells. Free Radical. *Biol Med.* 2001;31: 1509–1519.
17. Frankel A, Pabo C. Cellular uptake of the tat protein from human immunodeficiency virus. *Cell.* 1988;55:1189–1193.
18. Fawell S, Seery J, Daikh Y, Moore C, Chen LL, Pepinsky B, and Barsoum J. Tat-mediated delivery of heterologous proteins into cells. *Proc Natl Acad Sci U S A.* 1994;91:664–668.
19. Takenobu T, Tomizawa K, Matsushita M, Li ST, Moriwaki A, Lu YF, and Matsui H. Development of p53 protein transduction therapy using membrane-permeable peptides and the application to oral cancer cells. *Mol Cancer Ther.* 2002;1:1043–1049.
20. Inoue M, Tomizawa K, Matsushita M, Yun-Fei Lu, Yokoyama T, Yanai H, Takashima A, Kumon H, Matsui H. p53 protein transduction therapy: successful targeting and inhibition of the growth of the bladder cancer cells. *Eur Urol.* 2006;49:161–168.
21. Wu HY, Tomizawa K, Matsushita M, Lu YF, Li ST, Matsui H. Poly-arginine-fused calpastatin peptide, a living cell membrane-permeable and specific inhibitor for calpain. *Neurosci Res.* 2003;47:131–135.
22. Schwarze SR, Ho A, Vocero-Akbani A, Dowdy SF. In vivo protein transduction: delivery of a biologically active protein into the mouse. *Science.* 1999;285:1569–1572.
23. Green M, Loewenstein PM. Autonomous functional domains of chemically synthesized human immunodeficiency virus tat trans-activator protein. *Cell.* 1988;55:1179–1188.
24. Gustafsson AB, Sayen MR, Williams SD, Crow MT, Gottlieb RA. TAT protein transduction into isolated perfused hearts. *Circulation.* 2002;106: 735–739.
25. Asoh S, Ohsawa I, Mori T, Katsura K, Hiraide T, Katayama Y, Kimura M, Ozaki D, Yamagata K, Ohta S. Protection against ischemic brain injury by protein therapeutics. *PNAS.* 2002;99:17107–17112.
26. Matsushita M, Tomizawa K, Moriwaki A, Li ST, Terada H, Matsui H. A high-efficiency protein transduction system demonstrating the role of PKA in long-lasting long-term potentiation. *J Neurosci.* 2001;21: 6000–6007.
27. Matsushita M, Noguchi H, Lu YF, Tomizawa K, Michiue H, Li ST, Hirose K, Bonner-Weir S, Matsui H. Photo-acceleration of protein release from endosome in the protein transduction system. *FEBS Lett.* 2004;572: 221–226.
28. Matsui H, Tomizawa K, Lu YF, and Matsushita M. Protein Therapy: in vivo protein transduction by polyarginine (11R) PTD and subcellular targeting delivery. *Curr Protein Pept Sci.* 2003;4(2):151–157.
29. Wadia JS, Stan RV Dowdy SF. Transducible TAT-HA fusogenic peptide enhances escape of TAT-fusion proteins after lipid raft macropinocytosis. *Nat Med.* 2004;10:310–315.
30. Ülkan K, Ertugrul K, Gunnar PHD, Mathias B. Intravenous TAT-GDNF is protective after focal cerebral ischemia in mice. *Stroke.* 2003;34: 1304–1310.
31. Michiue H, Tomizawa K, Wei FY, Matsushita M, Lu YF, Ichikawa T, Tamiya T, Date I, and Matsui H. The NH2 terminus of influenza virus hemagglutinin-2 subunit peptides enhances the antitumor potency of polyarginine-mediated p53 protein transduction. *J Biol Chem.* 2005;280: 8285–8289.
32. Schwarze SR, Hruska KA, Dowdy SF. Protein transduction: unrestricted delivery into all cells? *Trends in Cell Biol.* 2000;10:290–295.
33. Kilic E, Dietz GPH, Hermann DM, Bähr M. Intravenous TAT–Bcl-X_L is protective after middle cerebral artery occlusion in mice. *Ann Neurol.* 2002;52:617–622.
34. Yamaguchi M, Zhou C-M, Heistad DD, Watanabe Y, Zhang JH. Gene Transfer of extracellular superoxide dismutase failed to prevent cerebral vasospasm after experimental subarachnoid hemorrhage. *Stroke.* 2004; 35:2512–2517.
35. Khurana VG, Meyer FB. Translational paradigms in cerebrovascular gene transfer. *J Cerebral Blood Flow Metab.* 2003;23:1251–1262.

Available online at www.sciencedirect.com
SCIENCE DIRECT
Experimental Neurology 199 (2006) 311–327
Experimental Neurology
www.elsevier.com/locate/yexnr

The high integration and differentiation potential of autologous neural stem cell transplantation compared with allogeneic transplantation in adult rat hippocampus

K. Muraoka *, T. Shingo, T. Yasuhara, M. Kameda, W. Yuan, H. Hayase, T. Matsui, Y. Miyoshi, I. Date

Department of Neurological Surgery, Okayama University Graduate School of Medicine, Dentistry, and Pharmaceutical Sciences, 2-5-1 Shikata-cho Okayama, 700-8558, Japan

Received 3 May 2005; revised 30 November 2005; accepted 1 December 2005
Available online 9 March 2006

Abstract

Cell therapy is thought to have a central role in restorative therapy, which aims to restore function to the damaged nervous system. The purpose of this study was to establish an autologous neural stem cell (NSC) transplantation model using adult rats and to compare survival, migration, and differentiation between this system and allogeneic NSC transplantation. Furthermore, we compared the immunologic response of the host tissue between autologous and allogeneic transplantation. NSCs were removed from the subventricular zone of adult Fischer 344 rats using stereotactic methods. NSCs were expanded and microinjected into normal hippocampus in the autologous brain. Allogeneic NSC (derived from adult Wistar rats) transplantation was performed using the same procedure, and hippocampal sections were analyzed immunohistologically 3 weeks post-transplantation. The cell survival and migration rate were higher for autologous transplantation than for allogeneic transplantation, and the neuronal differentiation rate in the autologous transplanted cells far exceeded that of allogeneic transplantation. Furthermore, there was less astrocyte and microglia reactivity in the host tissue of the autologous transplantation compared with allogeneic transplantation. These findings demonstrate that immunoreactivity of the host tissue strongly influences cell transplantation in the CNS as the autologous transplantation did not induce host tissue immunoreactivity; the microenvironment was essentially maintained in an optimal condition for the transplanted cells.

Introduction

Transplantation of neural stem cells (NSCs) is a key strategy for cell replacement therapy in the central nervous system (CNS) (Rossi and Cattaneo, 2002). The major limitation of this approach is the availability of donor tissue. Clinical studies concerning transplantation into the CNS have been based primarily on fetal brain tissue (Bjorklund and Lindvall, 2000; Lindvall, 2001). Approaches to bypass the shortage in donor tissue include in vitro expansion of NSCs by mitogen treatment (Ostenfeld et al., 2000; Reynolds and Weiss, 1992), ex vivo introduction of growth-stimulating oncogenes (Snyder et al., 1995), xeno-transplantation (Fink et al., 2000), enhancement of endogenous neurogenesis in adults (Kuhn et al., 1997), and attempts to recruit non-neural adult stem cells from other tissues (Brazelton et al., 2000; Mezey et al., 2000). Recent advances in adult-derived NSC technology provide an alternative method (Englund et al., 2002a,b; Zhang et al., 2003) to generate neural donor cells in unlimited quantities. Protocols have been established for the efficient generation of neural, glial, and neuronal-restricted precursors from adult rat subventricular zone (SVZ) (Garcia-Verdugo et al., 1998) and hippocampus (Lois and Alvarez-Buylla, 1993). After transplantation, adult-derived NSCs incorporate into the host CNS with subsequent differentiation to neurons or glia. Some issues remain, however, because the survival, integration, and neuronal differentiation rate of the transplanted NSCs are too low in the host CNS to accomplish functional recovery. In fact, only a small number of grafts integrate into the host CNS, and there is relatively low graft survival, limited synapse formation, and poorly regulated function (Dziewczapolski et al., 2003). Important factors that greatly affect graft cell fate include the microenvironment, which consists of endogenous local cues (Bernal and Peterson,

* Corresponding author. Fax: +81 86 227 0191.
E-mail address: ken-ichi@zj8.so-net.ne.jp (K. Muraoka).

0014-4886/$ - see front matter © 2005 Elsevier Inc. All rights reserved.
doi:10.1016/j.expneurol.2005.12.004

2004; Liu et al., 2003), and the host versus graft reaction. In particular, immunologic responses in the CNS are important. The CNS is continuously and effectively patrolled by the immune system (Cserr and Knopf, 1992). The healthy CNS is strictly regulated and has little ability to mount an immune response or process antigens (Aloisi et al., 1999); it does, however, have a well-organized innate immune reaction in response to allogeneic antigens and cerebral injury (Date et al., 1988; Date et al., 1991; Tambur, 2004). The immune reaction cannot be disregarded in the current allogeneic transplantation model (Wood et al., 1993). Moreover, although NSCs do not have antigenicity in the undifferentiated stage, major histocompatibility is expressed in the differentiation process during which antigenicity is acquired (McLaren et al., 2001; Widner and Brundin, 1993). The host astrocytes and microglia are the main immune components in the CNS (Aloisi et al., 1999). These cells proliferate and migrate into the graft, and immune interactions prevent full integration of the graft into the host with subsequent limitation of functional recovery (Tambur, 2004). We hypothesized that the optimal condition for NSC transplantation is autologous CNS. There is little information available about the behavior of adult-derived NSCs following autologous transplantation within the adult mammalian CNS. In the present study, same-strain NSC transplantation, i.e., syngeneic transplantation, was performed as a model of autologous transplantation and compared with allogeneic transplantation. The main aim of this study, however, was to return autologous NSCs, extracted from one brain and expanded in vitro, to the same brain, namely, to establish an autologous NSC transplantation model and to examine the effects of true autologous transplantation. It is thought that the tissue removal surgery induces changes in the host brain that influence graft survival. We observed the effects of autologous transplantation under such conditions. Allogeneic grafts were used for comparison in this experiment. Allogeneic grafts have low immunogenicity, despite the fact that they express major histocompatibility complex class I and costimulatory molecules (Odeberg et al., 2005). Consequently, if immunosuppressants were used in the present experiment, allogeneic transplantation might result in a comparable outcome compared with autologous transplantation because, in addition to immunosuppression, immunosuppressants have a neuroprotective effect. Compared with allogeneic grafts, factors related to the use of immunosuppressants will complicate examination of the influence of the tissue removal surgery. Immunosuppressants are not generally used in clinical autologous transplantation. Thus, in the present study, because immunosuppressants were not used, the difference between the two groups was limited to immunologic factors, and cell fate was compared. To facilitate allogeneic transplantation, however, it is important to inhibit the immunologic reaction of the host tissue. In cell therapy for diseases with a hereditary element, an allogeneic graft is possibly superior to an autologous graft. In contrast, autologous NSC transplantation can be used for traumatic or cerebrovascular injury in the CNS and has the advantage that immunologic response does not need to be considered. Furthermore, because there are no ethical issues, it will be easier to establish an autologous transplantation method for clinical application. Thus, we created an autologous transplantation model.

Materials and methods

Animals

Forty-four adult male Fischer 344 rats (220–240 g at the beginning of the studies; Clea, Japan) were used as hosts (20 rats for autologous NSC transplantation, 12 rats for allogeneic NSC transplantation, 12 rats for control), and 12 adult male Wistar rats were used as allogeneic graft donors. Animals were housed two per cage in a temperature- and humidity-controlled room that was maintained on a 12-h light/dark cycle and had free access to food and water. All animal procedures were performed in accordance with the guidelines approved by the institutional animal care and use committee of Okayama University. All efforts were made to minimize the number of animals used and their suffering.

Stereotactic removal of the SVZ tissue and NSC culture

All rats (Fischer 344 and Wistar rats) were deeply anesthetized with sodium pentobarbital (30 mg/kg, i.p.) and placed in a stereotactic instrument (Narishige, Inc. Tokyo, Japan). A midline skin incision was made in the skull, and a burr hole was drilled. A 16-gauge sheath (Terumo, Inc. Tokyo, Japan) attached to a syringe (1.0 ml) was slowly inserted into the cerebrum by applying gentle negative pressure, and the inner syringe was withdrawn. The sheath was then slowly withdrawn. The following coordinates were used; calculated from bregma: anterior–posterior = +1.5 mm; medial–lateral = +1.5 mm; depth = −4.0 mm. A piece of bone wax (W810, Ethicon, Sommerville, NJ) was used to seal the skull defect to prevent cerebrospinal fluid leakage. A cylindrical piece of tissue including the SVZ (approximate volume: 0.0047 μm^3) was transferred into phosphate-buffered saline (PBS) and cut into small pieces under a surgical microscope. Stereotactically removed adult rat SVZ-derived NSCs were prepared as described previously (Reynolds and Weiss, 1992; Shingo et al., 2001). Briefly, SVZ cells from adult rats were incubated with 1.4 μg/μl trypsin, 0.7 μg/μl hyaluronidase, and 0.2 μg/μl kynurenic acid for 15 min at 37°C and finally triturated using a fire-polished Pasteur pipette. Cells were seeded in Dulbecco's modified Eagle's medium/F12 (Invitrogen Corporation, Grand Island, NY) containing 0.6% glucose, 2 nM $NaHCO_3$, 0.5 mM HEPES, 100 μg/ml human apo-transferrin (Sigma Chemical Co., St. Louis, MO), 60 μM putrescine (Sigma), 20 nM progesterone (Sigma), 30 nM selenium chloride (Sigma), 25 μg/ml human insulin (Sigma), 2 μM L-glutamine, and 20 ng/ml epidermal growth factor (PeproTech EC, London, UK). Cells were grown in uncoated plastic flasks during the primary culture as free-floating clusters (neurospheres). The spheres were passaged by mechanical dissociation every 10 days and reseeded on Poly-HEME (2-hydroxyethyl methacrylate, Sigma)-coated flasks as a single-cell solution at a density of approximately 1×10^5 cells/ml into the culture media described

above (with 20 ng/ml epidermal growth factor). Neural stem/progenitor cell populations were obtained from neurospheres after at least two passages at 37°C in a humidified 5% CO_2 atmosphere.

Differentiation in vitro

Cell preparation

After two passages, each strain-derived neurosphere was mechanically triturated to produce a single-cell suspension. Cells were plated in the NSC media described above supplemented with 10% fetal bovine serum at a density of 1×10^5 cells/well on poly-D-ornithine and fibronectin-coated glass slides in 24-well plates (Nunc, Frankfurt, Germany). Cultures were maintained at 37°C in an atmosphere of 5% CO_2/95% air and 100% relative humidity. Ninety-six hours (h) after the initial plating (fourth day in vitro), the medium was removed and the cultures were analyzed.

Immunocytochemistry

Cells were fixed with 4% paraformaldehyde for 30 min and then washed three times for 5 min in PBS. They were incubated overnight at 4°C with an antibody directed against beta-tubulin (β-tubulin, mouse monoclonal IgG, 1:500, Sigma) with 10% normal goat serum (Vector Laboratories, Burlingame, CA). After several rinses in PBS, cells were incubated at room temperature (RT) for 30 min in donkey anti-mouse IgG Cy3 conjugate (1:1000, Sigma) and 4′,6-diamidino-2-phenylindole, dilactate (DAPI, 1:500, Molecular Probes, Eugene, OR). The cells were washed three times in PBS, mounted on albumin-coated slides, and embedded. Immunopositive neurons were quantified by counting and photographically documented. Immunoreactive cells were counted per randomly selected high power field view. The other series of cells were analyzed in the same way with an antibody directed against glial-fibrillary acidic protein (GFAP, 1:500 polyclonal IgG, BTI Inc. Stoughton, MA) and an antibody directed against O4 (mouse monoclonal IgM, 1:50, Chemicon International, Temecula, CA). Donkey anti-rabbit IgG AMCA conjugate (1:200, Chemicon) and donkey anti-rabbit IgG fluorescein isothiocyanate (FITC) conjugate (1:200, Chemicon) were used as secondary antibodies. Immunopositive cells were counted as described above. In control studies, the primary antibody was replaced with 10% normal goat serum in PBS. There was no immunoreactivity in these controls.

NSC transplantation in vivo

Cell preparation

Two different pre-labeling strategies were used to detect NSCs after transplantation. An adenovirus vector containing the gene encoding enhanced green fluorescent protein (GFP) was added to the growth medium at a multiplicity of infection of 160, 18 h prior to the transplantation. After cell expansion in vitro, the number of NSCs eventually reached 6.5×10^6 on average. Because the PFU value (PFU/ml) of purified adenovirus used in this study had already been determined (9.5×10^{11} PFU/ml), 160 times as many adenovirus vectors as the number of cells (1.04×10^9 PFU) was added (approximately 1 μl). Hoechst 33342 (5 μg/ml) was added to the culture medium 2 h prior to transplantation. Thereafter, GFP- and Hoechst-33342-labeled SVZ cells were resuspended by trypsinization and collected by centrifugation ($70 \times g$, 7 min). Single-cell suspensions were prepared in PBS. Nucleated SVZ cells were counted using a cytometer to ensure an adequate cell number for transplantation (approximately 1×10^5 NSCs in 1 μl PBS).

Autologous NSC transplantation

Recipient Fischer 344 rats that had previously had tissue removed from their right hemisphere were deeply anesthetized with sodium pentobarbital (30 mg/kg, i.p.) and placed in a stereotactic instrument (Narishige, Japan). Using a 5-μl Hamilton syringe (Hamilton 87900, Hamilton, Reno NV), 1 μl of the cell suspension (1×10^5/μl) was injected over a 10-min period into the left side of the hippocampus (intact hemisphere) at the following coordinates; calculated from bregma: anterior–posterior = −3.5 mm; medial–lateral = −2.0 mm; depth = −3.0 mm (Paxinos and Watson, 1998). After implantation, the cannula was left in place for an additional 5 min and slowly withdrawn (1 mm/min).

Allogeneic NSC transplantation

Allogeneic grafts were removed from Wistar rats and cultured as described above. Recipient Fischer 344 rats underwent the same tissue removal procedure as the rats used for autologous NSC transplantation in the right hippocampus before transplantation. Allogeneic NSC transplantation was performed in the left hippocampus 30 days after the tissue removal procedure. No immunosuppressive drugs were used.

Control animals

Control animals (Fischer 344 rats) underwent the same tissue removal procedure as the rats in the other groups. PBS (1 μl) was injected into the left hippocampus 30 days after the tissue removal procedure.

Tissue processing

Four recipient rats in the autologous NSC transplantation group were sacrificed 1 and 2 weeks post-transplantation to evaluate the migration of transplanted cells. The other 36 recipient rats were sacrificed 3 weeks post-transplantation. All rats were anesthetized with an overdose of pentobarbital (70 mg/kg), transcardially perfused with cold PBS, followed by 250 ml of cold 4% paraformaldehyde in 0.1 M phosphate buffer. The brains were rapidly removed and postfixed in 4% paraformaldehyde overnight at 4°C, before being transferred

to 30% sucrose in 0.1 M phosphate buffer for cryoprotection. Coronal sections (14 μm thick) were cut on a freezing microtome for quantitative analyses.

Immunohistochemistry

Sections collected on slides were incubated overnight at 4°C with an anti-GFP antibody (rabbit polyclonal, 1:500, MBL International, Woburn, MA; mouse monoclonal, 1:200, Molecular Probes), an anti-NeuN antibody (mouse monoclonal, 1:100, Chemicon), an anti-Doublecortin (Dcx) antibody (guinea pig polyclonal, 1:2000, Chemicon), an anti-GFAP antibody (rabbit polyclonal, 1:500, Sigma), or an anti-Iba1 antibody (rabbit polyclonal, 1:150, Wako Inc, Osaka, Japan) with 10% normal goat serum (Vector Laboratories). After several rinses in PBS, sections were incubated for 1 h in donkey anti-rabbit IgG FITC conjugate (1:500, Jackson ImmunoResearch Laboratories, West Grove, CA), donkey anti-mouse IgG FITC conjugate (1:500, Jackson), biotinylated donkey anti-mouse (1:1000, Jackson), donkey anti-guinea pig (1:500, Jackson), or donkey anti-rabbit (1:500, Jackson) IgG. After several rinses in PBS, the sections were incubated for 45 min in Cy3 conjugate streptavidin (1:2000, Jackson). All nuclei were stained with DAPI (1:1000, Molecular Probes) in PBS for 5 min followed by washing with PBS. The sections for CD4, CD8, or caspase-3 were pretreated with 0.3% H_2O_2 in methanol for 30 min and incubated with 10% normal goat serum in PBS for 1 h at RT to block non-specific binding. The sections were incubated with 100-fold dilution of an anti-CD4 antibody (mouse monoclonal, Serotec Inc., London, UK), an anti-CD8 antibody (mouse monoclonal, Serotec), or an anti-caspase-3 antibody (goat-polyclonal, Santa Cruz Biotechnology Inc, Santa Cruz, CA) in PBS. They were incubated with biotinylated anti-mouse IgG (1:200), anti-goat IgG (1:100) for 1 h at RT, followed by incubation in an avidin–biotin complex solution (Vector Laboratories) for 1.5 h at RT. Sections were visualized by a 3,3′-diaminobenzidine kit (D5905, Sigma). The sections were dehydrated with graded ethanol series and then passed through pure xylene. In the control studies, the primary antibody was replaced with 10% normal goat serum in PBS. There was no immunoreactivity in these controls.

Quantification of cell survival, differentiation, and migration distance

Few transplanted cells were identified in the section which was 500 μm or more away from the transplant site. Therefore, it was evaluated about the surviving cell located within the 490 μm from the transplanted site. A 1-in-7 series of coronal sections (14 μm thick) in the range of 490 μm rostral and 490 μm caudal to the transplant coordinates (A–P: −3.6, total 10 sections) was collected. All GFP-positive transplanted cells resided in this range. Dead cells and red blood cells produce auto-fluorescence under a fluorescence microscope. We, therefore, counted cells before phenotype-specific immunostaining to distinguish green (GFP)-single-positive surviving cells from auto-fluorescent dead cells. Cells that were green fluorescent (+)/red fluorescent (−) were considered to be surviving cells. In contrast, green/red double positive cells were excluded as dead cells or red blood cells. Furthermore, apoptotic cells were detected by caspase-3 immunostaining and taken into account when determining survival rate. For counting caspase-3-positive cells, we regarded a deeply DAB-stained nucleus or cell body as a positive cell. The estimated number of the total surviving cells was calculated by multiplying the number of GFP-positive surviving cells by 7 to take into account that the sections were collected as a 1-in-7 series. The number of GFP (surviving)-, NeuN/GFP (maturely neuronal differentiated)-, Dcx/GFP (committed to differentiate into neurons)-, and GFAP/GFP-positive (glial differentiated) cells was counted. The distance the transplanted cells migrated from the core of the graft was measured using StereoInvestigator software (MicroBrightfield, Williston, VT). For the medio-lateral axis, we measured the distance from the core of the cluster to the most distant grafts.

Quantification of caspase-3-positive apoptotic cells

The number of caspase-3-positive apoptotic cells was counted in the same range as the range which counted the number of surviving cells. The numbers of samples were nine samples, respectively. The reason for counting apoptotic cells is as the following. When apoptotic cells are observed with a fluorescence microscope, they are auto-fluorescent. Although auto-fluorescent apoptotic cells were fully eliminated when counting the number of GFP-positive surviving cells, they might be counted to the number of surviving cells accidentally. Then, by counting the number of apoptotic cells, it was examined whether comparison of the number of total surviving cells would be affected when apoptotic cells were accidentally added to a surviving cell.

Morphologic evaluation

Quantification of GFAP- or Iba1-positive cells

The two areas occupied by GFAP-positive astrocytic elements or Iba1-positive microglial cells were quantitatively determined (Shetty et al., 2004) per unit area of tissue in the vicinity of the needle tract between the CA1 and superior pyramidal cell layer of the dentate gyrus to assess reactions of the host tissue against the penetration injury and the area adjacent to the cluster of transplanted NSCs (the cluster area) to assess the graft vs. host reaction. The comparable site in PBS-injected animals was also analyzed as a control. Every seventh 14-μm-thick coronal tissue section was sampled for evaluation in each group. Quantification was performed using Scion Image software (Scion Corporation, Frederick, ML). The microscopic image (40× objective) was transferred to the computer by focusing on the appropriate area of the immunostained section with an Olympus BX50 microscope equipped with a digital video camera system (DP70, Olympus Inc., Tokyo, Japan). The images from different animals were digitized in gray scale with identical parameters using the digital camera and saved as TIFF

files for subsequent measurements in Scion Image. Images opened in Scion Image display two-dimensional arrays of pixels (picture elements), ranging in value from 0 to 255. Scion Image displays pixels with a value of 0 as white and those with a value of 255 as black. Measurements of sections from each group were performed in a blinded manner using experimental codes. The tissue was coded such that the animal group was not known during the measurements; however, sections that came from the same animal could be identified. For measurements in each image, the binary image of the GFAP- or Iba1-immunopositive elements was created by selecting a threshold value that keeps all the GFAP- or Iba1-immunopositive structures, but not the background staining, in the binary image. The final binary image was carefully cross-checked with the original gray-scale image by alternating the two images on the computer screen. The area occupied by the GFAP- or Iba1-immunopositive structures in the binary image was then measured by selecting the Analyze Particles command in the Scion Image program. In this way, the area of individual GFAP- or Iba1-immunopositive structures in the selected field was measured in every section, and the summed area of all particles was stored for further calculations and statistical analyses. The measurements were later converted into the area of GFAP- or Iba1-immunopositive elements per square micrometer. The values for GFAP- or Iba1-immunopositive elements were calculated separately for each animal using data from every seventh section before the means and standard errors were determined for the total number of animals.

Semiquantitative evaluation of CD4/CD8-positive lymphocyte infiltration

Sections processed for CD4 and CD8 immunostaining were semiquantitatively evaluated microscopically under bright-field illumination on renumbered slides, as described previously with modifications for application to the hippocampus (Duan et al., 1996). Each section was rated by two independent investigators and classified into one of the following categories: (0) no specific immunostaining in the graft area; (1) few positive cells, distributed as scattered single cells or clustered in a few small patches in or around the graft; (2) several positive cells distributed as single cells or clustered in multiple, prominent patches around the grafts; (3) dense immunostaining of the graft area and a large number of positive cells in and around the graft; and (4) highly dense immunostaining of the whole graft area and a very large number of positive cells in and around the graft or positive cells were widespread, occupying more than one-third of the grafted hippocampus.

Measurement of pro-inflammatory cytokine production by enzyme-linked immunosorbent assay (ELISA)

Three weeks after transplantation, the rats were killed by cervical dislocation; the brains were rapidly removed, sliced into 2-mm sections, and both the transplanted and vehicle-injected hippocampus were punched out (diameter: 3 mm), snap-frozen in liquid nitrogen, and stored at −80°C for subsequent extraction and quantification for interleukin-1β (IL-1β) or tumor necrosis factor α (TNFα) by ELISA. For optimal extraction of proteins, the tissue was homogenized on ice in phosphate buffer containing protease inhibitors (Completemini, Roche, Mannheim, Germany) at pH 7.4. Homogenates were centrifuged (12,000 × g) for 10 min at 4°C, and the supernatants were removed and assayed in duplicate immediately, along with calibrated cytokine standards. The sensitivities of these ELISA kits were equal to or better than 25.6 pg/ml for IL-1β and 31 pg/ml for TNFα. Protein concentrations of the samples were analyzed using a commercially available protein assay according to the manufacturer's instructions (IL-1β: RPN2743, TNFα: RPN2744, Amersham Biosciences, NJ), and results were expressed as pg/mg protein.

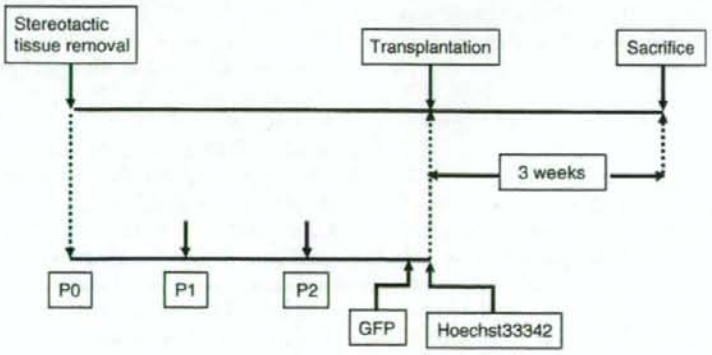

Fig. 1. Experimental design of autologous NSC transplantation. First, SVZ tissue was removed from adult rat brain by stereotactic surgery. NSCs were cultured selectively for 30 days in vitro. Cells were passaged twice and expanded sufficiently for transplantation surgery. The rats that underwent tissue removal operation were bred during this period. After labeling with GFP using adenovirus infection and Hoechst 33342, the cultured NSCs were transplanted into the autologous hippocampus. The rats were sacrificed 3 weeks post-transplantation for histologic examination.

Statistical analysis

The data obtained were evaluated statistically using analysis of variance (ANOVA) and post hoc Scheffe's F test. A P value of less than 0.05 was considered to be statistically significant.

Results

Establishment of autologous NSC transplantation model

We first established a culture method for preparing an adequate number of NSCs from stereotactically removed tissue. Fig. 1 shows the experimental design. First, SVZ tissue was removed from adult rat brain by stereotactic surgery. NSCs were cultured selectively for 30 days in vitro. Cells were passaged twice and expanded sufficiently for transplantation surgery. The rats that underwent tissue removal operation were bred during this period. After labeling with GFP using adenovirus infection and Hoechst 33342, the cultured NSCs were transplanted into the autologous hippocampus. The rats were sacrificed 3 weeks post-transplantation for histologic examination.

Cell properties of stereotactically removed NSCs

We evaluated the donor cell properties of the two rat strains (Fischer 344 and Wistar). Stereotactically removed adult SVZ-derived NSCs were cultured for 30 days just prior to transplantation. The neurospheres were passaged every 10 days. The increase in the NSC population at each stage of passage is shown in Fig. 2A. After the first passage, the NSC population was $2.2 \pm 0.1 \times 10^4$ in Fischer 344 and $2.3 \pm 0.2 \times 10^4$ in Wistar rats. After the second passage, the NSC population was $10.5 \pm 0.6 \times 10^4$ in Fischer 344 and $10.2 \pm 0.5 \times 10^4$ in Wistar rats. Finally, $6.4 \pm 1.7 \times 10^6$ cells from Fischer 344 rats and $6.2 \pm 1.5 \times 10^6$ cells from Wistar rats were obtained just prior to transplantation. NSCs had sufficient proliferative potential, and there was no significant difference between the two strains (first passage: $P = 0.797$, second passage: $P = 0.703$, just prior to transplantation: $P = 0.655$). Cell phenotype was then assayed before transplantation using phenotype-specific antibodies. Table 1 shows the rate of differentiation into each phenotype for each strain. Immunostaining for the neuronal marker β-tubulin revealed that $2.3 \pm 0.3\%$ (Fischer 344) and $2.1 \pm 0.1\%$ (Wistar) of the cultured NSCs were β-tubulin-positive, indicating that cultured NSCs could differentiate into neurons. The in vitro neuronal differentiation rate was not significantly different between the two strains. NSCs had the potential to differentiate into three lineages (neuron, astrocyte, oligodendrocyte). We confirmed that both strains had almost the same degree of proliferative capacity and differentiation potential for the three lineages (Table 1). Fig. 2B shows a brain specimen 4 weeks after stereotactic tissue removal, corresponding to the brain condition right before the rats underwent transplantation surgery. For tissue removal, the rostral dorso-lateral corner of the lateral ventricle, where NSCs are abundantly located, was considered the most important area. Fig. 2B shows that the removed parenchymal tissue included important region of SVZ. Although little bleeding was observed from the depths of the cavity formed immediately after tissue removal, it stopped spontaneously. The cavity resulting from the tissue removal was small, and there was neither a marked degree of atrophy nor a brain shift due to swelling. Specifically, under direct vision, the contralateral hemisphere was not grossly influenced. The GFP labeling rate was $25.2 \pm 1.3\%$ in Fischer 344 rats and $26.1 \pm 1.7\%$ in Wistar rats. There was no significant difference between the two strains (mean values ± SE, $P = 0.71$).

Survival and migration of the transplanted NSCs

NSCs were transplanted into the dentate gyrus in the hippocampus of adult rats to assess whether cultured NSCs survive, migrate, and differentiate in response to endogenous cues. The grafts were placed within the hilum of the dentate gyrus. Overall graft survival and cell distribution were analyzed by GFP gene expression. Three weeks post-transplantation, the total number of surviving NSCs in the autologous group was

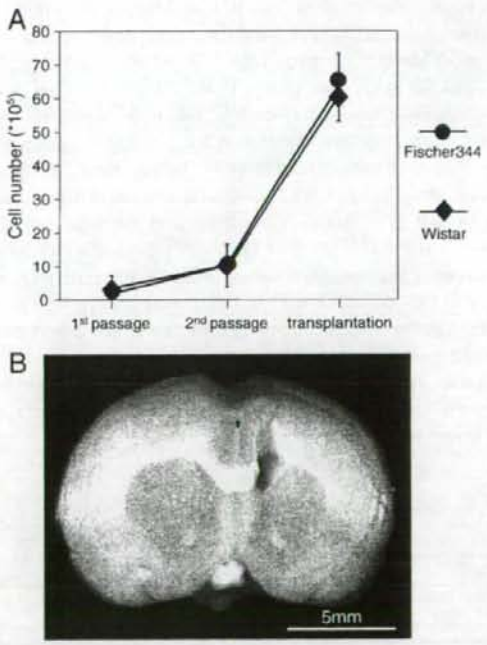

Fig. 2. (A) NSC expansion in vitro. Stereotactically removed adult SVZ-derived NSCs were cultured for 30 days just prior to transplantation. The neurospheres were passaged twice every 10 days. NSCs had sufficient proliferative potential, and there was no significant difference between the two strains (1st passage: $P = 0.797$, 2nd passage: $P = 0.703$, just prior to transplantation: $P = 0.655$).The figure shows mean values ± SE. (B) Brain specimens 4 weeks after stereotactic tissue removal. This condition corresponds to the brain condition right before transplantation surgery was performed. In tissue removal, the rostral dorso-lateral corner of lateral ventricle, where NSCs were abundantly located, was considered the most important area to extract NSCs. This figure shows that the dorsal half of a lateral ventricle was extracted. The biopsy-induced cavity was small and did not grossly influence surrounding structures.

Table 1
The rate of differentiation to each phenotype in vitro in each strain

	F344	Wistar	P
β-tubulin	2.3 ± 0.3	2.1 ± 0.1	0.52
GFAP	49.2 ± 4.9	52.3 ± 2.1	0.55
O4	0.9 ± 0.2	0.8 ± 0.2	0.58

Immunostaining for the neuronal marker β-tubulin, astrocyte marker GFAP, and oligodendrocyte marker O4 revealed that the NSCs had the potential to differentiate into three lineages after two passages. The in vitro differentiation rate was not significantly different for each phenotype between the two strains. Table shows mean values ± SE.

5129.8 ± 243.0 (5.1% ± 0.2%), significantly greater than that in the allogeneic group (3430.7 ± 328.6: 3.4% ± 0.3%; Table 2). Some of the GFP-positive cells remained in a cluster just below the granule cell layer (GCL) where the transplanted cells had been injected and the round-shaped morphology of these cells was unchanged. Many GFP-positive cells were outside the cluster and had spread in all directions by 1 week post-transplantation (Fig. 3A). At 2 weeks post-transplantation, cells that migrated outside the cluster were located mainly in the subgranular zone (SGZ) and distributed laterally along the SGZ (Fig. 3B). Finally, the transplanted autologous NSCs reached a maximum outside the dentate gyrus at 3 weeks post-transplantation (Fig. 3C). At 3 weeks, the number of NSCs that migrated away from the transplantation site was 1113.2 ± 52.7 (migration rate: 21.7 ± 2.7% of total surviving cells; Table 2) in the autologous group. In the allogeneic group, there were significantly fewer cells (466.6 ± 56.8, 13.6 ± 4.9%, Table 2). The maximum migration distance in the autologous group was 19.2 ± 0.65 μm, which tended to be further than that in the allogeneic group (17.3 ± 0.62 μm), although the difference was not significant ($P = 0.062$). Cells located in the SGZ extended processes into the GCL (Fig. 4A). These cells had morphologically neuronal features. In addition, some of the cells migrated ventrally to the ventricular wall and integrated into the host tissue (Fig. 4B). On the other hand, some grafts moved dorsally through the needle tract, migrated tangentially, and distributed along the GCL in the CA1 region (Fig. 4C). Some of those cells were Dcx-positive and tended to differentiate into neurons in the CA1 region (Figs. 4D, E, F).

Table 2
Survival, migration, and migration distance of transplanted NSCs

	Autologous	Allogeneic	P
Total number of surviving cells	5129.8 ± 243.0*	3430.7 ± 328.6	<0.001
Number of NSCs migrated away from graft site (%)	1113.2 ± 52.7* (21.7 ± 2.7)	466.6 ± 56.8	<0.001
Maximum migration distance (mm)	19.2 ± 0.65	17.3 ± 0.62	0.062

At 3 weeks post-transplantation, the total number of surviving NSCs in the autologous group was significantly higher than that in the allogeneic group. The number of NSCs that migrated from transplantation site was significantly greater in the autologous group than in allogeneic group. The migration rate was significantly greater in the autologous group than in the allogeneic group. The maximum migration distance in the autologous group tended to be greater than that in the allogeneic group, although the difference was not significant. Table shows mean values ± SE.

* $P < 0.001$.

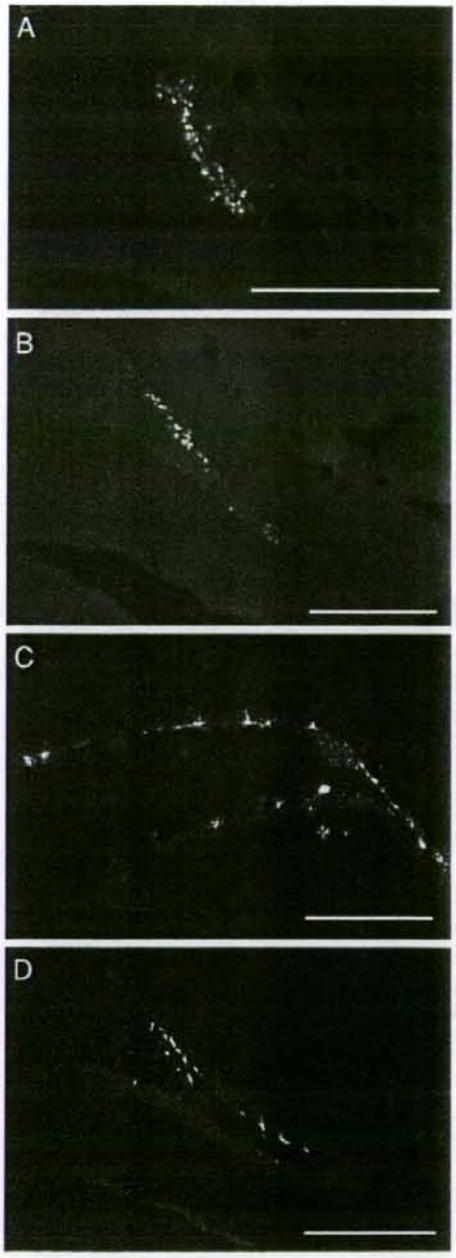

Fig. 3. Time course of NSC migration. Immunohistologic examination indicated that many GFP-positive cells survived and migrated in the hippocampus. (A) GFP-positive cells that were outside of the transplanted NSC cluster spread in all directions 1 week post-transplantation. (B) At 2 weeks post-transplantation, the cells that migrated out from the cell cluster were mainly distributed laterally along the SGZ. (C) Finally, the transplanted autologous NSCs moved along the SGL and reached a maximum outside of the dentate gyrus at 3 weeks post-transplantation (A, B, C: autologous transplantation). (D) Only a small number of cells survived in the allogeneic transplantation. Scale bar = 1.0 mm.

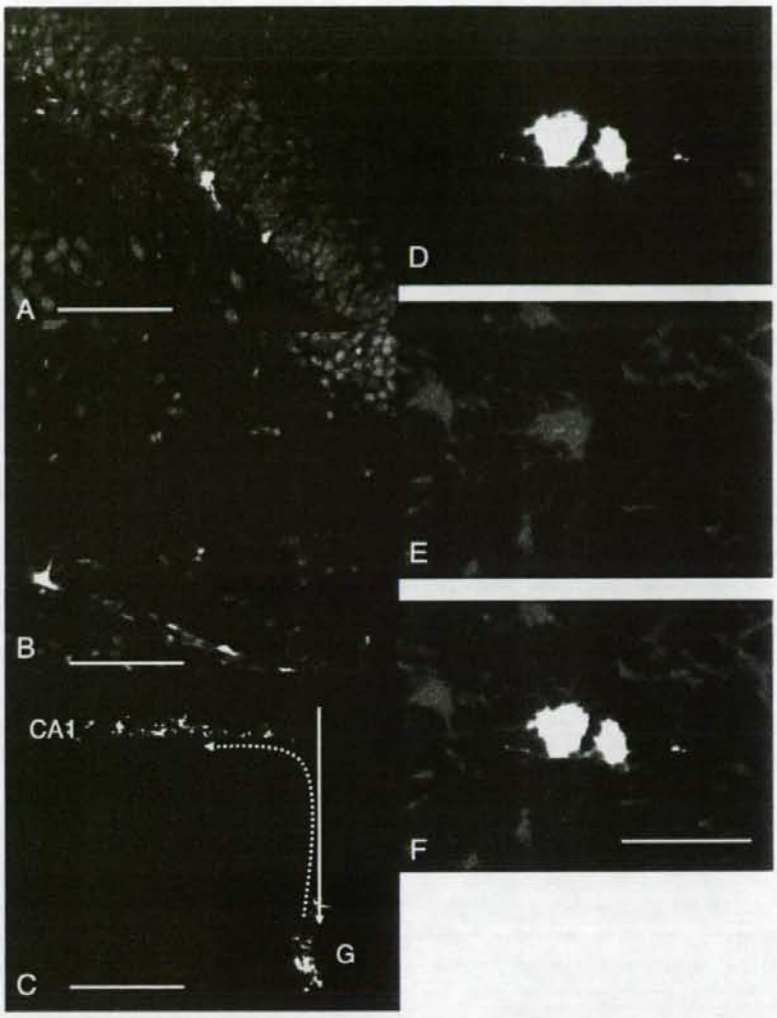

Fig. 4. Migration of autologous GFP-positive cells. (A) The transplanted NSCs located in the SGZ extended processes into the GCL (scale bar = 200 μm). (B) Some cells migrated ventrally and reached the ventricular wall where they integrated in the host tissue (scale bar = 200 μm). Panels A and B represent double staining of NeuN (red; Cy3) and nuclear (blue; DAPI). The merged image became pink in color. (C) Some of the grafts (GFP-positive green cells) moved in the dorsal direction through the needle tract, migrated tangentially, and arranged along the GCL in the CA1. (dotted line: migration pathway, full line: needle tract, scale bar = 1.0 mm). (D) GFP-positive cells that migrated into the CA1. (E) Some of the migrating cells were Dcx-positive in the CA1. (F) Merged image of Panels D and E, some of the GFP-positive cells expressed Dcx and tended to differentiate into neurons in the CA1 region (scale bar = 50 μm). (A–F: autologous transplantation) Green: GFP, blue: DAPI, red: NeuN in Panels A and B, Dcx in Panels E and F. (For interpretation of the references to colour in this figure legend, the reader is referred to the web version of this article.)

Morphologic analyses and cell differentiation inside and outside the graft cluster

To examine whether the transplanted NSCs differentiated into neurons or astrocytes within the host dentate gyrus, double immunostaining of the mature neuronal markers (NeuN) and GFP, immature neurogenic marker (Dcx) and GFP, glial cell marker (GFAP) and GFP, and microglia marker (Iba1) and GFP was performed. Migrating cells rapidly lost their round shape and were ramified in both groups, suggesting good integration into the host tissue and some degree of morphologic differentiation. The total number of differentiated NSCs (%) (Dcx-positive, NeuN-positive, and GFAP-positive) of the total surviving cells was 23.3 ± 1.1% in the autologous group (Table 3). This was a significantly higher number than that in the allogeneic group (20.2 ± 1.9%, Table 3). For the grafts outside the cluster (i.e., migrated away from the cluster), the differentiation rate was 52.5 ± 3.9% in the autologous group and 47.9 ± 5.6% in the allogeneic group (Table 3). These differentiation rates were significantly higher than that in the cells that remained at the transplantation site (8.5 ± 0.7% in the autologous group, 10.2 ± 1.3% in the allogeneic group, Table 3). On the other hand, the majority of cells remaining at the transplantation site did not express a

Table 3
The each and total rates of neuronal or glial differentiated NSCs (Dcx-positive, NeuN-positive, and GFAP-positive) among the surviving cells

		Autologous	Allogeneic	P
Total survived cells (%)	Dcx	9.3 ± 0.6**	4.7 ± 0.6	<0.001
	NeuN	3.3 ± 0.2**	1.6 ± 0.1	<0.001
	GFAP	10.7 ± 0.5	13.9 ± 1.3*	0.023
	Total rates	23.3 ± 1.1*	20.2 ± 1.9	0.043
NSCs migrated away from the graft site (%)	Dcx	26.5 ± 2.0*	19.5 ± 2.4	0.022
	NeuN	11.2 ± 0.9**	5.8 ± 0.7	<0.001
	GFAP	14.8 ± 1.0	22.6 ± 2.5**	<0.001
	Total rates	52.5 ± 3.9	47.9 ± 5.6	0.28
NSCs remaining at graft site (%)	Dcx	0.0	0.0	NA
	NeuN	0.0	0.0	NA
	GFAP	8.5 ± 0.7	10.2 ± 13	0.15
	Total rates	8.5 ± 0.7	10.2 ± 1.3	0.15

The total rates of differentiated NSCs among total number of surviving cells were significantly greater in the autologous group than in the allogeneic group. A large number of grafted cells that migrated away from the transplantation site had differentiated. In contrast, grafted cells that remained at the transplantation site had a low differentiation rate. There is no significant difference between two groups in each division. However, with respect to the differentiation rate to each of the three phenotypes, the Dcx-positive and NeuN-positive rate of total surviving cells was significantly higher in the autologous group than in the allogeneic group. On the contrary, the astroglial differentiation rate (GFAP-positive) was lower in the autologous group than in the allogeneic group. Among the cells that migrated outside of the cluster, the Dcx-positive and NeuN-positive rate were significantly higher in the autologous group than in the allogeneic group. In contrast, the differentiation rate of GFAP/GFP-positive cells was significantly lower in the autologous group than in the allogeneic group. Among the cells that remained at the transplantation site, only GFAP-positive cells were detected. The astroglial differentiation rate in the autologous group tended to be lower than that in the allogeneic group. Table shows mean values ± SE.
NA: not available.
* $P = 0.05$.
** $P < 0.001$.

phenotype-specific marker and did not demonstrate morphologic changes. The few grafts that expressed phenotype-specific marker were GFAP-positive cells located in the periphery of the graft cluster.

Neuronal and glial differentiation of autologous and allogeneic grafts

Dcx/GFP dual-positive cells located in the SGZ and extended processes into the GCL (Figs. 5A, B, C). Some transplanted cells that moved into the GCL expressed the mature neuronal marker NeuN (Figs. 5D, E, F). NeuN/GFP dual-positive cells were spindle-shaped like endogenous neurons located at the periphery and extended axon-like processes. Strongly GFP-immunoreactive NSCs, however, did not express NeuN or Dcx. These cells were highly branched and ramified with a glia-like morphology. Some of them were GFAP/GFP dual-positive and located in the SGZ (Figs. 5G, H, I). The neuronal differentiation rate (sum of Dcx and NeuN) of the total number of surviving cells was 12.6 ± 0.8% in the autologous group and 6.3 ± 0.7% in the allogeneic group (Table 3). All the cells that were neuronally differentiated migrated away from the cell cluster and located in the SGZ or the GCL. Immunohistologic examination revealed that there were no neuronally differentiated cells inside the cluster, and a large proportion of grafts inside the cluster were not immunoreactive for any of the antigens tested and remained poorly differentiated or undifferentiated. These results indicated that a suitable environment for inducing neuronal differentiation, called the neuronal niche (Doetsch, 2003, Doetsch et al., 2002), was not maintained in areas where massive clusters were located but was maintained in areas distant from the graft cluster where transplanted NSCs migrated, even if they were in the same dentate gyrus. Furthermore, when the evaluation was limited to the cells outside of the cluster, the differentiation rates of Dcx/GFP-positive cells and NeuN/GFP-positive cells were significantly higher in the autologous group (26.5 ± 2.0% and 11.2 ± 0.9%) than in the allogeneic group (19.5 ± 2.4% and 5.8 ± 0.7%; Dcx: $P = 0.022$, NeuN: $P < 0.01$, Table 3). In contrast, the differentiation rate of GFAP/GFP-positive cells was significantly lower in the autologous group (14.8 ± 1.0%) than in the allogeneic group (22.6 ± 2.5%; Table 3, $P < 0.001$). None of the transplanted NSCs was Iba1-positive.

Extent of astrocytic and microglial reaction after NSC transplantation

Astrocytes in the vicinity of the needle tract had thicker and longer processes (Fig. 6A). The quantification of GFAP-positive astrocytic elements revealed that needle-insertion-induced reactions increased GFAP-positive structures and were larger in the cell transplantation group than in the control group (Fig. 7A, allogeneic vs. control: $P = 0.003$, autologous vs. control: $P = 0.037$); there was no significant difference between the autologous and allogeneic groups ($P = 0.55$). Quantification of Iba1-positive microglial elements revealed no difference between the three groups in the needle tract (Fig. 7B, allogeneic vs. control: $P = 0.09$, autologous vs. control: $P = 0.29$, allogeneic vs. autologous: $P = 0.71$). Although the host astrocytes in the cluster area exhibited little change in the control group (Fig. 6B), astrocytes clearly proliferated and had swelled bodies and thicker processes in the cell transplantation groups (Figs. 6C, D, E). The antigen-related immunologic rejection in the cluster area induced an increase in the number of microglia. Microglia in the cluster areas also exhibited swollen soma and shorter and stouter processes (Figs. 6F, G, H). The extent of astrocytic and microglial hypertrophy in the cluster areas was significantly larger in the allogeneic transplantation group than in the control group (Figs. 7C, D). Quantification of GFAP and Iba1-immunoreactive elements revealed that the allogeneic graft induced the greatest increases in the host tissue (areas adjacent to the cluster of transplanted cells) in the three groups. Moreover, an ANOVA to examine the effects of the immunologically different (autologous or allogeneic) graft transplantations revealed that the allogeneic transplantation induced a significantly larger reaction in host astrocytes and microglia in the cluster areas compared with autologous transplantation (Figs. 7C, D).

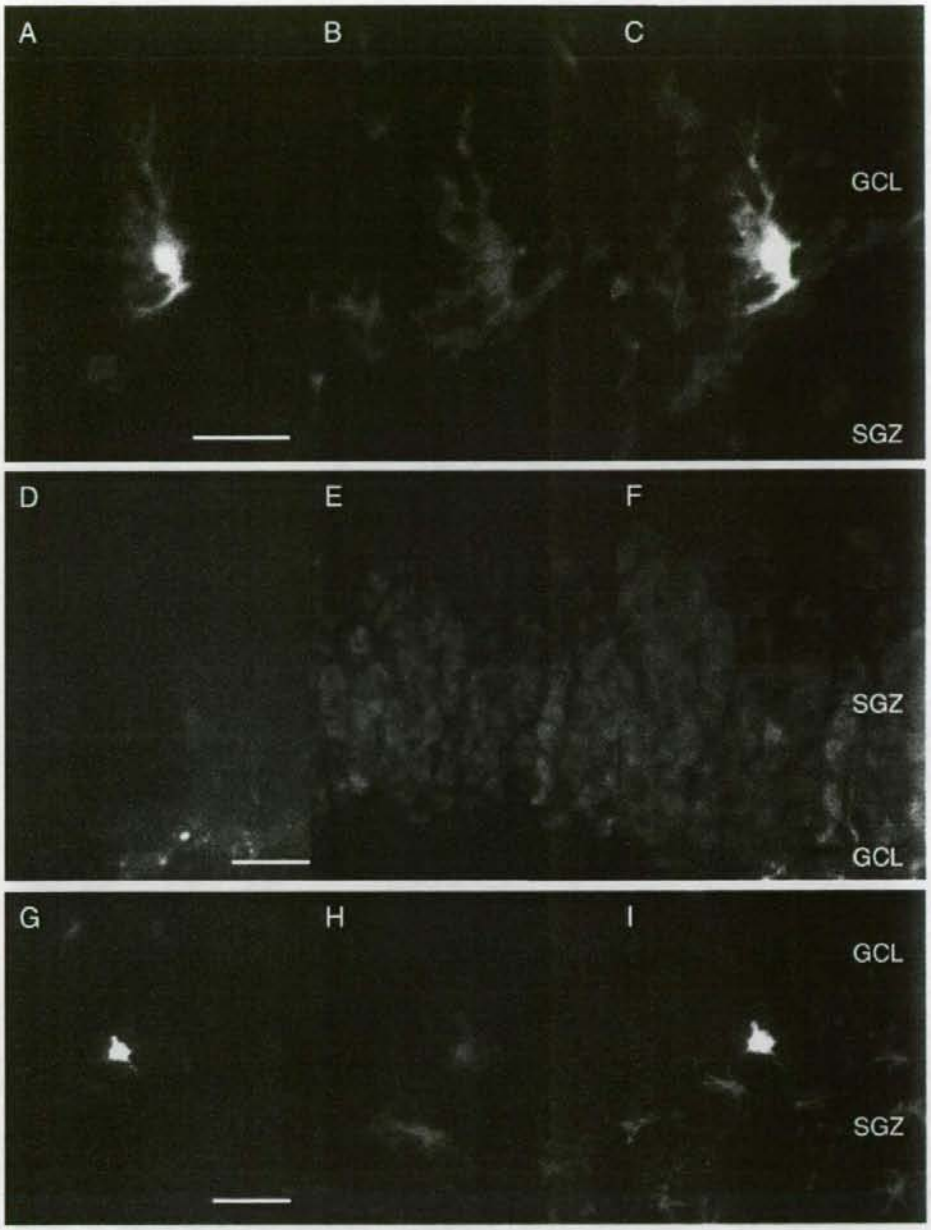

Fig. 5. Differentiation of autologous grafts. (A, B, and C) Dcx (red)/GFP-positive cells located in the SGZ and extended processes into the GCL. Panel C is the merged image of panels A and B. (D, E, and F) Some transplanted cells that moved into the GCL expressed mature neuronal marker NeuN. NeuN (red)/GFP-positive cells were spindle-shaped like endogenous neurons located in the circumference and extended axon-like processes. Panel F is the merged image of panels D and E. (G, H, and I) GFAP (red)/GFP-positive cells located in the SGZ. These cells were highly branched and ramified with a glia-like morphology. Panel I is the merged image of panels G and H. (A–I: autologous transplantation) Green: GFP, blue: DAPI, scale bar = 50 μm. (For interpretation of the references to colour in this figure legend, the reader is referred to the web version of this article.)

Immune response and induction of pro-inflammatory cytokines IL-1β and TNFα

NSC transplantation induced an immunologic response and induction of pro-inflammatory cytokines in the brain, as indicated by the infiltration of CD4-positive and CD8-positive lymphocytes in the cluster and the increased IL-1β and TNFα concentrations (Fig. 9). Both CD4-positive and CD8-positive lymphocytes were localized to the graft area. CD4 immunohistochemical staining, which marked rounded cells with a

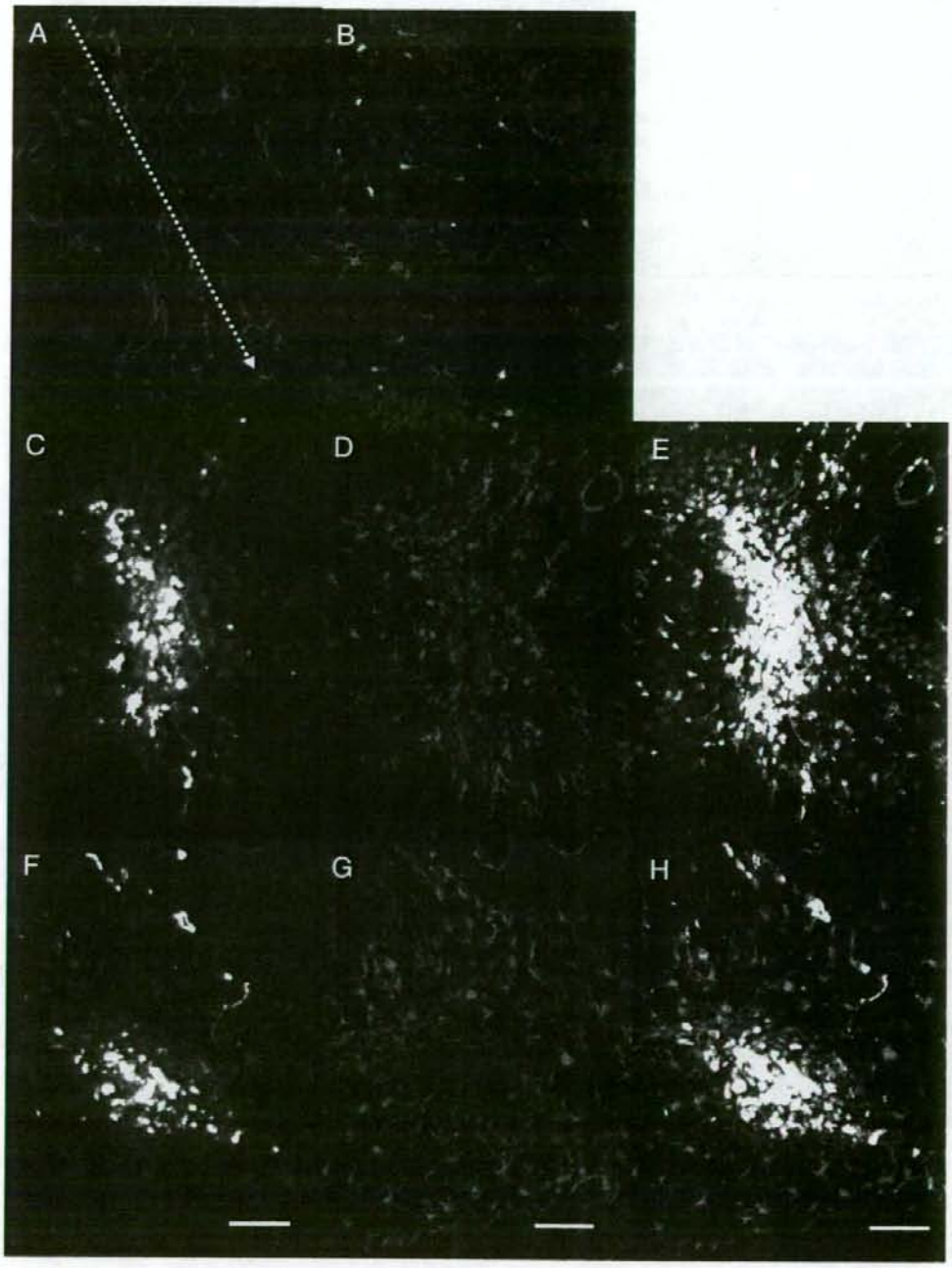

Fig. 6. Glial reaction after NSC transplantation. (A) The GFAP-positive astrocytic reactions (red) in the vicinity of the needle tract exhibited thicker and longer processes in the allogeneic group (dotted line: needle tract). (B) There was almost no host astrocytic response in the dentate hilum in the control group. (C and D) In areas immediately adjacent to the cluster of transplanted NSCs (green) in the dentate hilum, the astrocytes (red) were gathered around the cluster and exhibited thicker and longer processes. Panel E is the merged image of panels C and D. (F and G) The areas adjacent to the cluster of transplanted cells exhibited increased numbers of microglia (red) induced by the graft (green)-related host tissue reaction. Microglia exhibited swollen soma and shorter and stouter processes. Panel H is the merged image of panels F and G. (C–H: allogeneic transplantation) blue: DAPI, scale bar = 200 μm. (For interpretation of the references to colour in this figure legend, the reader is referred to the web version of this article.)

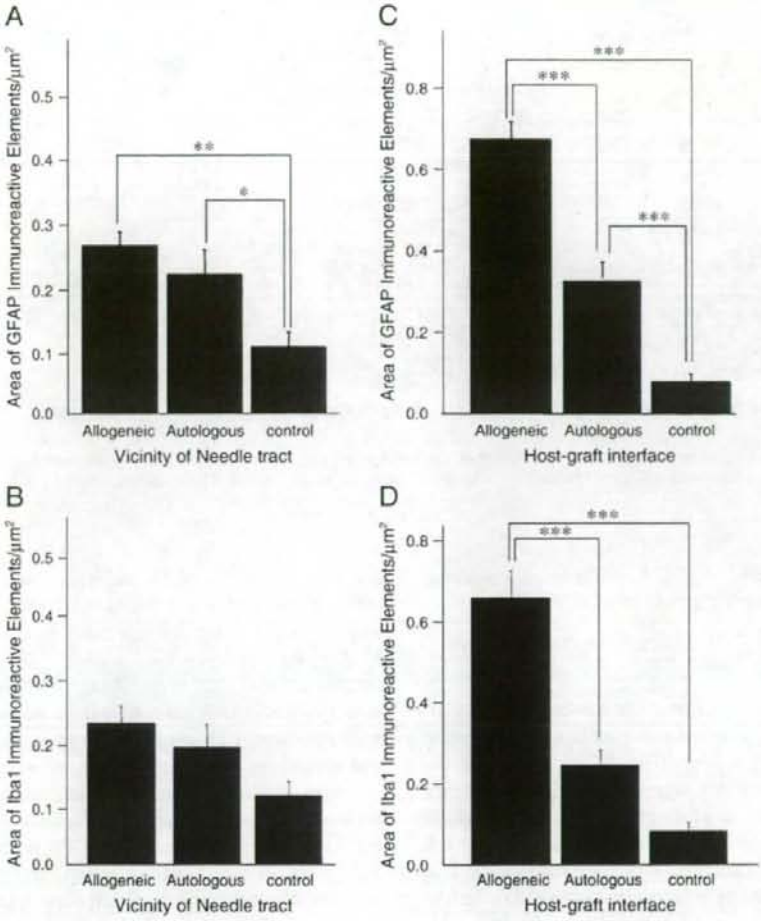

Fig. 7. Quantification of GFAP-immunoreactive astrocytic elements revealed that needle-insertion-induced increases in GFAP-immunoreactive structures in the areas between the CA1 and the superior pyramidal cell layer were larger in the NSC transplantation group than in the control group and there was no significant difference between autologous and allogeneic transplantation (A, allogeneic vs. control: $P = 0.032$, autologous vs. control: $P = 0.037$, allogeneic vs. autologous: $P = 0.55$). Quantification of Iba1-immunoreactive microglial elements revealed that needle-insertion-induced increases in Iba1-immunoreactive structures in the areas between the CA1 region and the superior pyramidal cell layer were comparable across the three groups (B, allogeneic vs. autologous: $P > 0.7$, allogeneic vs. control: $P > 0.09$, autologous vs. control: $P > 0.2$). The extent of astrocytic hypertrophy in the cluster areas was significantly different among the three groups. The graft-related host astrocyte reaction in the dentate hilum of the autologous transplantation was significantly less than in that of the animals receiving allogeneic grafts (C, allogeneic vs. control: $P < 0.001$, autologous vs. control: $P < 0.001$, allogeneic vs. autologous: $P < 0.001$). Quantification of Iba1-immunoreactive microglial elements in the cluster areas revealed that the allogeneic transplantation induced larger increases in Iba1-immunoreactive structures than autologous transplantation in the host tissue (D, $P < 0.001$). There was a significantly larger graft-related host microglial reaction in the dentate hilum of the allogeneic transplantation group than in the control group, however, there was no difference between the autologous and control groups (D, allogeneic vs. control: $P < 0.001$, autologous vs. control: $P = 0.08$). Error bar: SE. * indicates $\ll P < 0.05$, ** indicates $P < 0.01$, *** indicates $P < 0.001$.

typical lymphocytic morphology, revealed that cells were located at the periphery of the grafted cell clusters (Fig. 8A). In contrast, the CD8-positive lymphocytes infiltrated the cell cluster (Fig. 8B). The results of the semiquantitative evaluation revealed that the degree of lymphocyte aggregation and infiltration tended to increase in order of control, autologous, and allogeneic transplantation (Figs. 9A, B). The concentration of IL-1β was significantly higher in allogeneic transplantation than in autologous transplantation (Fig. 9C; 1107.7 ± 47.4 and 865.4 ± 77.9 pg/mg, respectively, $P = 0.033$). On the other hand, there was no significant difference between autologous transplantation and control groups (Fig. 9C; 660 ± 45.8 pg/mg, $P = 0.107$). The concentration of TNFα tended to be greater in the allogeneic transplantation group than in the autologous transplantation and control groups. There was no significant difference in TNFα between the three groups (Fig. 9D 550.8 ± 80.0, 405.8 ± 35.4, and 383.2 ± 29.8 pg/mg, respectively,

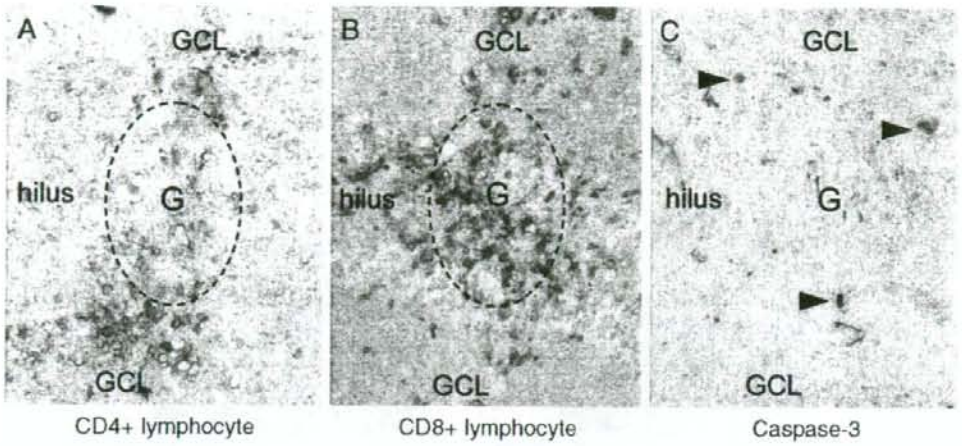

Fig. 8. Immune reaction. (A) CD4 immunohistochemical staining, which marked rounded cells with a typical lymphocytic morphology, revealed that cells were located at the periphery of grafted cell cluster. (B) The CD8-positive lymphocytes infiltrated the cell cluster. (C) Almost all caspase-3-positive cells were located in the periphery of the graft cluster.

allogeneic vs. autologous: $P = 0.173$, allogeneic vs. control: $P = 0.139$, autologous vs. allogeneic: $P = 0.960$).

Detection of apoptotic cells

An increase in caspase-3 activity is an early marker of apoptosis. Almost all caspase-3-positive cells were located in the periphery of the graft clusters (Fig. 8C). We counted the number of cells that were darkly stained by caspase-3 antibody as apoptotic cells. The number of apoptotic cells was very small (allogeneic: 17.1 ± 3.3, autologous: 12.6 ± 2.5, mean $\pm$ SE, n.s.). The reason for the small number was presumed to be that caspase-3 appears transiently and disappears quickly in the apoptotic cascade.

Discussion

The present study demonstrated that SVZ tissue could be removed from an adult rat brain and the NSCs expanded from the biopsy of a small region. Furthermore, a cell suspension of the expanded NSCs could be successfully microinjected into the hippocampus of the same rat. That is, we established an autologous NSC transplantation model in the adult rat. The autologous NSC transplantation resulted in a high rate of graft survival and neuronal differentiation in the host tissue as compared with allogeneic transplantation. Immunohistologic examination of the host tissue indicated that astrocytes and microglia induced host inflammatory and immunologic responses and were greatly involved in graft survival and integration.

Survival and migration

The presumed survival rate of total surviving cells was $5.1 \pm 0.2\%$ in the autologous group and $3.4 \pm 0.3\%$ in the allogeneic group. This survival rate was not as high as in previous reports of NSC transplantation (Consiglio et al., 2004; Fricker et al., 1999; Le Belle et al., 2004). Underestimation of the survival rate might be due to down-regulation of the GFP adenovirus vector. Furthermore, it is also speculated that the host tissue recognized the adenovirus vector as foreign and caused an immunologic reaction in grafts because many CD8-positive lymphocytes were observed in and around the graft cluster. Because the adenovirus infection rate was $25.3 \pm 2.4\%$ in the present study, if surviving GFP-negative cells were included, the actual survival rate would be expected to be approximately 20.4% in the autologous group and 13.6% in the allogeneic group. Thus, the survival rate is actually comparable with the reports mentioned above. The number of detectable grafted cells might increase if lentivirus or other methods that have a high labeling rate are used for cell labeling (Englund et al., 2002a,b; Falk et al., 2002). Physiologic stress and mechanical damage during the series of transplantation operations at the time of transplant are reported to be the most important causes of graft death (Cameron et al., 1998, Shetty et al., 2004). That is, many of the disappearing cells probably become apoptotic and degenerate soon after the transplantation. Moreover, dead cells, which presented as auto-fluorescent, were observed in the graft cluster, suggesting that apoptotic cell death continued and led to a reduction in the number of surviving cells after transplantation due to the host inflammatory reaction that occurred following the transplantation surgery. Secondary neuronal damage reduces graft viability and induces delayed cell death, largely due to genetic mechanisms, as evidenced by apoptosis (Kernie et al., 2001). The inflammatory reaction of the host tissue against operative injury was confirmed by the immunohistochemical examination of reactive astrocytes and microglia in the control group. As part of the inflammatory response, pro-inflammatory cytokines (e.g., TNFα, IL-1β, and IFNγ) are synthesized by resident cells (Mirza et al., 2004; Tambur, 2004). On the other hand, as a result of

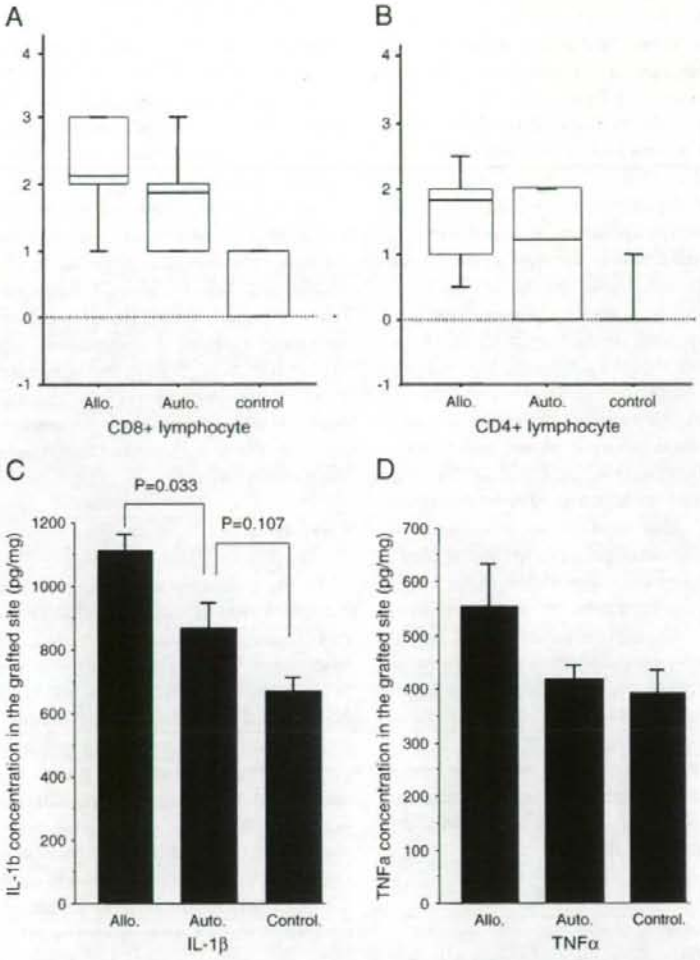

Fig. 9. Diagram showing infiltration of immune cells in the dentate gyrus. Semiquantitative rating of the infiltration of CD8-positive lymphocytes (A) and CD4-positive lymphocytes (B) in the transplanted dentate gyrus, showing the medians, 25th and 75th percentiles, and 10th and 90th percentiles. (C) There was a significantly higher concentration of IL-1β in the allogeneic group than in the autologous group ($P = 0.033$). On the other hand, there was no significant difference between the autologous and control groups ($P = 0.107$). (D) There was a greater concentration of TNFα in the allogeneic group than in the autologous and control groups. There was no significant difference between the three groups in the concentration of TNFα (550.8 ± 80.0, 405.8 ± 35.4 and 383.2 ± 29.8 pg/mg, respectively, allogeneic vs. autologous: $P = 0.173$, allogeneic vs. control: $P = 0.139$, autologous vs. allogeneic: $P = 0.960$).

transplantation surgery, various neurotrophic cytokines, such as brain-derived neurotrophic factor, nerve growth factor, and neurotrophin-3 (Shetty et al., 2004), are produced by resident cells. Such host inflammatory and injurious reactions could alter the neurogenic environment of the dentate gyrus to be either optimal or unsuitable for neuronal differentiation (Ben-Hur et al., 2003; Lu et al., 2005; Wong et al., 2004). Reactive astrocytes and microglia form a glial scar around the graft clusters. Such morphologic transformation also physically restricts graft migration and reduces viability. Thus, it is important to minimize the reaction of the host tissue when performing transplantation surgery. To overcome these problems, it might be necessary to optimize the environment of the injured host tissue for cell survival and integration.

Neuronal differentiation

Neurogenesis occurs in the hippocampus in the adult rat brain (Feng et al., 2001; Shors et al., 2001). The microenvironment in the adult hippocampus supports neurogenesis and is suitable for the neuronal differentiation of transplanted NSCs and is therefore called a "neurogenic niche". The present study demonstrated that autologous SVZ-derived NSCs differentiated into neurons after transplantation in the autologous hippocampus. As far as grafts that migrated away from the transplantation site, the differentiation rate of the grafted cells was high (autologous: 53.0 ± 3.1%, allogeneic: 47.9 ± 3.6%). In contrast, in grafts that remained at the transplantation site, the differentiation rate was low (autologous: 8.5 ± 0.7%, allogeneic:

10.2 ± 1.3%). In other words, the host inflammatory and immunologic reactions were strong and changed the original host neurogenic microenvironment at the transplantation site. Such a microenvironment would not be suitable for graft cell differentiation. In contrast, in the area where migrating cells located, the original host neurogenic condition could be maintained and the grafts differentiated at a high rate. Thus, the reason why the neuronal differentiation rate was higher in the autologous group than in the allogeneic group is that the host microenvironment is maintained in the state nearer to the original neuronal niche in the autologous group. On the other hand, in the allogeneic group, the neuronal differentiation rate decreases in the microenvironment formed as a result of the immunologic reaction. Specifically, the difference between the two groups is not due to apoptosis of differentiated cells by direct immunologic attack, but the neuronal differentiation rate itself. It is thought that the host neurogenic niche changes, and, as a result, the neuronal differentiation rate tends to decrease and the glial differentiation rate tends to rise. Therefore, at the transplantation site, the glial differentiation rate was higher in the allogeneic group than in the autologous group (Monje et al., 2003). For successful restoration and regeneration of the CNS, it is necessary to reproduce the intricate conditions to control migration and raise the neuronal differentiation rate of grafts. Intrinsic signals form restorative conditions that guide neuronal differentiation in non-neurogenic regions in a pathologic environment, such as ischemia (Tanaka et al., 2004), Parkinson's disease, and traumatic injury (Hallbergson et al., 2003). Further studies must be performed to elucidate the mechanisms that guide neurogenesis and to develop manipulation techniques to promote full integration of grafts, depending not only on intrinsic factors but also on extrinsic factors.

Immunologic aspects

Our results indicated that the autologous grafts were superior to the allogeneic grafts with respect to the potential to survive, migrate, and differentiate to neurons. Immunohistologic examination revealed that proliferation of reactive astrocytes, microglia, and lymphocytes was more active in the allogeneic group than in the autologous group. Microglia, which act as antigen-presenting cells (Aloisi et al., 1999), recognized an alloantigen in the allogeneic graft and gathered around the graft periphery. Furthermore, various signals that are released from microglia induce proliferation and migration of reactive astrocytes and CD4-positive and CD8-positive lymphocytes (Tambur, 2004). These cells might affect each other, accelerate immune responses, and produce various cytokines, such as IL-1β, IFNγ, TNFα, and TGFβ (Monje et al., 2003). These substances might reduce the viability of allogeneic grafts and seriously influence allogeneic cell fate (Vallieres et al., 2002). Antigenicity is increased by various inflammatory cytokines produced by host reactive cells (Tambur, 2004). As described above, the more peripheral the graft cells in the graft cluster, the more frequently they expressed phenotype-specific antigens. Consequently, it was assumed that these cells acquire antigenicity and are then attacked by immunologic reaction, which leads to apoptosis (McLaren et al., 2001). We detected apoptotic cells that accumulated caspase-3 in the cell body in the periphery of the graft cluster, confirming our speculation. Although NSCs express costimulatory molecules (Imitola et al., 2004; Ling et al., 1998) and acquire antigenicity, it is unclear whether the acquisition of antigenicity will be promoted by cytokines and how strongly alloantigens are enhanced by host inflammation and immunologic reaction in vivo (Odeberg et al., 2005). These questions require further study. The use of steroids to induce an adequate immunosuppressive effect is problematic because steroids suppress neuronal differentiation (Cameron et al., 1998). In CNS cell therapy, which requires a rigorously controlled microenvironment (i.e., the neurogenic niche) (Doetsch, 2003), the autologous NSC transplantation might be an advantageous excellent method because there is no need to take immunologic responses into consideration and because there is minimal alteration of the original host microenvironment.

Conclusion

In the present study, we established an autologous NSC transplantation model using adult rats. The survival, migration, and neuronal differentiation rates were excellent in the autologous NSC transplantation as compared with allogeneic NSC transplantation. These results suggest that autologous NSCs are excellent candidate donors for cell therapy in the CNS. Future studies examining use of immunosuppressants, graft survival at later time points, transplantation into non-neurogenic regions, and applications for disease models are necessary in order to apply autologous NSC transplantation in clinical practice. Moreover, it is important to elucidate the mechanisms by which various extracellular signals guide neuronal differentiation and to better control the restorative conditions in various neurodegenerative disorders.

Acknowledgments

We thank Hideki Wakimoto for the photographic work and Masako Arao and Tomoko Ujihashi for technical assistance. This work was supported in part by Grants-in-Aid for Scientific Research from the Ministry of Education, Culture, Sports, Science, and Technology, Japan; and by a Grant for the project for realization of regenerative medicine from the Ministry of Education, Culture, Sports, Science, and Technology.

References

Aloisi, F., Ria, F., Columba-Cabezas, S., Hess, H., Penna, G., Adorini, L., 1999. Relative efficiency of microglia, astrocytes, dendritic cells and B cells in naive CD4+ T cell priming and Th1/Th2 cell restimulation. Eur. J. Immunol. 29, 2705–2714.

Ben-Hur, T., Ben-Menachem, O., Furer, V., Einstein, O., Mizrachi-Kol, R., Grigoriadis, N., 2003. Effects of proinflammatory cytokines on the growth, fate, and motility of multipotential neural precursor cells. Mol. Cell. Neurosci. 24, 623–631.

Bernal, G.M., Peterson, D.A., 2004. Neural stem cells as therapeutic agents for age-related brain repair. Aging Cell. 3, 345–351.
Bjorklund, A., Lindvall, O., 2000. Cell replacement therapies for central nervous system disorders. Nat. Neurosci. 3, 537–544.
Brazelton, T.R., Rossi, F.M., Keshet, G.I., Blau, H.M., 2000. From marrow to brain: expression of neuronal phenotypes in adult mice. Science 290, 1775–1779.
Cameron, H.A., Tanapat, P., Gould, E., 1998. Adrenal steroids and *N*-methyl-D-aspartate receptor activation regulate neurogenesis in the dentate gyrus of adult rats through a common pathway. Neuroscience 82, 349–354.
Consiglio, A., Gritti, A., Dolcetta, D., Follenzi, A., Bordignon, C., Gage, F.H., Vescovi, A.L., Naldini, L., 2004. Robust in vivo gene transfer into adult mammalian neural stem cells by lentiviral vectors. Proc. Natl. Acad. Sci. U. S. A. 101, 14835–14840.
Cserr, H.F., Knopf, P.M., 1992. Cervical lymphatics, the blood–brain barrier and the immunoreactivity of the brain: a new view. Immunol. Today 13, 507–512.
Date, I., Kawamura, K., Nakashima, H., 1988. Histological signs of immune reactions against allogeneic solid fetal neural grafts in the mouse cerebellum depend on the MHC locus. Exp. Brain Res. 73, 15–22.
Date, I., Felten, S.Y., Felten, D.L., 1991. The nigrostriatal dopaminergic system in MPTP-treated mice shows more prominent recovery by syngeneic adrenal medullary graft than by allogeneic or xenogeneic graft. Brain Res. 545, 191–198.
Doetsch, F., 2003. A niche for adult neural stem cells. Curr. Opin. Genet. Dev. 13, 543–550.
Doetsch, F., Petreanu, L., Caille, I., Garcia-Verdugo, J.M., Alvarez-Buylla, A., 2002. EGF converts transit-amplifying neurogenic precursors in the adult brain into multipotent stem cells. Neuron 36, 1021–1034.
Duan, W.M., Brundin, P., Grasbon-Frodl, E.M., Widner, H., 1996. Methylprednisolone prevents rejection of intrastriatal grafts of xenogeneic embryonic neural tissue in adult rats. Brain Res. 712, 199–212.
Dziewczapolski, G., Lie, D.C., Ray, J., Gage, F.H., Shults, C.W., 2003. Survival and differentiation of adult rat-derived neural progenitor cells transplanted to the striatum of hemiparkinsonian rats. Exp. Neurol. 183, 653–664.
Englund, U., Bjorklund, A., Wictorin, K., Lindvall, O., Kokaia, M., 2002a. Grafted neural stem cells develop into functional pyramidal neurons and integrate into host cortical circuitry. Proc. Natl. Acad. Sci. U. S. A. 99, 17089–17094.
Englund, U., Fricker-Gates, R.A., Lundberg, C., Bjorklund, A., Wictorin, K., 2002b. Transplantation of human neural progenitor cells into the neonatal rat brain: extensive migration and differentiation with long-distance axonal projections. Exp. Neurol. 173, 1–21.
Falk, A., Holmstrom, N., Carlen, M., Cassidy, R., Lundberg, C., Frisen, J., 2002. Gene delivery to adult neural stem cells. Exp. Cell Res. 279, 34–39.
Feng, R., Rampon, C., Tang, Y.P., Shrom, D., Jin, J., Kyin, M., Sopher, B., Miller, M.W., Ware, C.B., Martin, G.M., Kim, S.H., Langdon, R.B., Sisodia, S.S., Tsien, J.Z., 2001. Deficient neurogenesis in forebrain-specific presenilin-1 knockout mice is associated with reduced clearance of hippocampal memory traces. Neuron 32, 911–926.
Fink, J.S., Schumacher, J.M., Ellias, S.L., Palmer, E.P., Saint-Hilaire, M., Shannon, K., Penn, R., Starr, P., VanHorne, C., Kott, H.S., Dempsey, P.K., Fischman, A.J., Raineri, R., Manhart, C., Dinsmore, J., Isacson, O., 2000. Porcine xenografts in Parkinson's disease and Huntington's disease patients: preliminary results. Cell Transplant 9, 273–278.
Fricker, R.A., Carpenter, M.K., Winkler, C., Greco, C., Gates, M.A., Bjorklund, A., 1999. Site-specific migration and neuronal differentiation of human neural progenitor cells after transplantation in the adult rat brain. J. Neurosci. 19, 5990–6005.
Garcia-Verdugo, J.M., Doetsch, F., Wichterle, H., Lim, D.A., Alvarez-Buylla, A., 1998. Architecture and cell types of the adult subventricular zone: in search of the stem cells. J. Neurobiol. 36, 234–248.
Hallbergson, A.F., Gnatenco, C., Peterson, D.A., 2003. Neurogenesis and brain injury: managing a renewable resource for repair. J. Clin. Invest. 112, 1128–1133.
Imitola, J., Comabella, M., Chandraker, A.K., Dangond, F., Sayegh, M.H., Snyder, E.Y., Khoury, S.J., 2004. Neural stem/progenitor cells express costimulatory molecules that are differentially regulated by inflammatory and apoptotic stimuli. Am. J. Pathol. 164, 1615–1625.
Kernie, S.G., Erwin, T.M., Parada, L.F., 2001. Brain remodeling due to neuronal and astrocytic proliferation after controlled cortical injury in mice. J. Neurosci. Res. 66, 317–326.
Kuhn, H.G., Winkler, J., Kempermann, G., Thal, L.J., Gage, F.H., 1997. Epidermal growth factor and fibroblast growth factor-2 have different effects on neural progenitors in the adult rat brain. J. Neurosci. 17, 5820–5829.
Le Belle, J.E., Caldwell, M.A., Svendsen, C.N., 2004. Improving the survival of human CNS precursor-derived neurons after transplantation. J. Neurosci. Res. 76, 174–183.
Lindvall, O., 2001. Parkinson disease. Stem cell transplantation. Lancet 358, S48 (Suppl.).
Ling, V., Munroe, R.C., Murphy, E.A., Gray, G.S., 1998. Embryonic stem cells and embryoid bodies express lymphocyte costimulatory molecules. Exp. Cell Res. 241, 55–65.
Liu, C.Y., Westerlund, U., Svensson, M., Moe, M.C., Varghese, M., Berg-Johnsen, J., Apuzzo, M.L., Tirrell, D.A., Langmoen, I.A., 2003. Artificial niches for human adult neural stem cells: possibility for autologous transplantation therapy. J. Hematother. Stem Cell Res. 12, 689–699.
Lois, C., Alvarez-Buylla, A., 1993. Proliferating subventricular zone cells in the adult mammalian forebrain can differentiate into neurons and glia. Proc. Natl. Acad. Sci. U. S. A. 90, 2074–2077.
Lu, Y.Z., Lin, C.H., Cheng, F.C., Hsueh, C.M., 2005. Molecular mechanisms responsible for microglia-derived protection of Sprague–Dawley rat brain cells during in vitro ischemia. Neurosci. Lett. 373, 159–164.
McLaren, F.H., Svendsen, C.N., Van der Meide, P., Joly, E., 2001. Analysis of neural stem cells by flow cytometry: cellular differentiation modifies patterns of MHC expression. J. Neuroimmunol. 112, 35–46.
Mezey, E., Chandross, K.J., Harta, G., Maki, R.A., McKercher, S.R., 2000. Turning blood into brain: cells bearing neuronal antigens generated in vivo from bone marrow. Science 290, 1779–1782.
Mirza, B., Krook, H., Andersson, P., Larsson, L.C., Korsgren, O., Widner, H., 2004. Intracerebral cytokine profiles in adult rats grafted with neural tissue of different immunological disparity. Brain Res. Bull. 63, 105–118.
Monje, M.L., Toda, H., Palmer, T.D., 2003. Inflammatory blockade restores adult hippocampal neurogenesis. Science 302, 1760–1765.
Odeberg, J., Piao, J.H., Samuelsson, E.B., Falci, S., Akesson, E., 2005. Low immunogenicity of in vitro-expanded human neural cells despite high MHC expression. J. Neuroimmunol. 161, 1–11.
Ostenfeld, T., Caldwell, M.A., Prowse, K.R., Linskens, M.H., Jauniaux, E., Svendsen, C.N., 2000. Human neural precursor cells express low levels of telomerase in vitro and show diminishing cell proliferation with extensive axonal outgrowth following transplantation. Exp. Neurol. 164, 215–226.
Paxinos, G., Watson, G., 1998. The Rat Brain in Stereotaxic Coordinates. Academic Press, Spiral Bound, New York.
Reynolds, B.A., Weiss, S., 1992. Generation of neurons and astrocytes from isolated cells of the adult mammalian central nervous system. Science 255, 1707–1710.
Rossi, F., Cattaneo, E., 2002. Opinion: neural stem cell therapy for neurological diseases: dreams and reality. Nat. Rev., Neurosci. 3, 401–409.
Shetty, A.K., Rao, M.S., Hattiangady, B., Zaman, V., Shetty, G.A., 2004. Hippocampal neurotrophin levels after injury: relationship to the age of the hippocampus at the time of injury. J. Neurosci. Res. 78, 520–532.
Shingo, T., Sorokan, S.T., Shimazaki, T., Weiss, S., 2001. Erythropoietin regulates the in vitro and in vivo production of neuronal progenitors by mammalian forebrain neural stem cells. J. Neurosci. 21, 9733–9743.
Shors, T.J., Miesegaes, G., Beylin, A., Zhao, M., Rydel, T., Gould, E., 2001. Neurogenesis in the adult is involved in the formation of trace memories. Nature 410, 372–376.
Snyder, E.Y., Taylor, R.M., Wolfe, J.H., 1995. Neural progenitor cell engraftment corrects lysosomal storage throughout the MPS VII mouse brain. Nature 374, 367–370.
Tambur, A.R., 2004. Transplantation immunology and the central nervous system. Neurol. Res. 26, 243–255.
Tanaka, R., Yamashiro, K., Mochizuki, H., Cho, N., Onodera, M., Mizuno, Y., Urabe, T., 2004. Neurogenesis after transient global ischemia in the

adult hippocampus visualized by improved retroviral vector. Stroke 35, 1454–1459.
Vallieres, L., Campbell, I.L., Gage, F.H., Sawchenko, P.E., 2002. Reduced hippocampal neurogenesis in adult transgenic mice with chronic astrocytic production of interleukin-6. J. Neurosci. 22, 486–492.
Widner, H., Brundin, P., 1993. Sequential intracerebral transplantation of allogeneic and syngeneic fetal dopamine-rich neuronal tissue in adult rats: will the first graft be rejected? Cell Transplant 2, 307–317.
Wong, G., Goldshmit, Y., Turnley, A.M., 2004. Interferon-gamma but not TNF alpha promotes neuronal differentiation and neurite outgrowth of murine adult neural stem cells. Exp. Neurol. 187, 171–177.
Wood, M.J., Sloan, D.J., Dallman, M.J., Charlton, H.M., 1993. Specific tolerance to neural allografts induced with an antibody to the interleukin 2 receptor. J. Exp. Med. 177, 597–603.
Zhang, R.L., Zhang, L., Zhang, Z.G., Morris, D., Jiang, Q., Wang, L., Zhang, L.J., Chopp, M., 2003. Migration and differentiation of adult rat subventricular zone progenitor cells transplanted into the adult rat striatum. Neuroscience 116, 373–382.

Available online at www.sciencedirect.com

SCIENCE DIRECT

Surgical Neurology 65 (2006) 167 - 169

SURGICAL NEUROLOGY

www.surgicalneurology-online.com

Technique

Transient memory disturbance after removal of an intraventricular trigonal meningioma by a parieto-occipital interhemispheric precuneus approach: Case report

Koji Tokunaga, MD[a,*], Takashi Tamiya, MD[b], Isao Date, MD[a]

[a]*Department of Neurological Surgery, Okayama University Graduate School of Medicine, Dentistry and Pharmaceutical Sciences, Okayama 700-8558, Japan*

[b]*Department of Neurological Surgery, Faculty of Medicine, Kagawa University, Kagawa 700-8558, Japan*

Received 15 December 2004; accepted 13 June 2005

Abstract

Background: Pitfalls in a parieto-occipital interhemispheric precuneus approach for the ventricular trigonal region of a dominant hemisphere have been rarely reported. We described a case with memory disturbance after surgery using this approach.

Case Description: A 57-year-old, right-handed woman complained of numbness of the lower extremities and underwent magnetic resonance imaging, which incidentally demonstrated a trigonal meningioma in the left lateral ventricle with a maximal diameter of 4 cm. The patient's preoperative neurologic examination was normal. The tumor was successfully removed by a parieto-occipital interhemispheric approach with an incision of the left precuneus cortex. Postoperative motor, sensory, and visual functions were normal; however, recent memory disturbance developed, which gradually resolved in the following 3 months.

Conclusions: An interhemispheric precuneus approach is a useful alternative to trigonal tumors with few surgical complications, but postoperative memory disturbance can be one pitfall of this procedure.

Keywords: Meningioma; Memory deficits; Intraventricular neoplasms; Operative surgical procedures

1. Introduction

Intraventricular meningiomas commonly arise in the trigone, and various surgical approaches to this region have been reported [2,4-9,11-13]. Among these, a parieto-occipital interhemispheric precuneus approach is a good alternative to preserve neurologic functions, particularly in the dominant hemisphere [5,6,9,13], but its pitfalls have been rarely described. We report a patient with trigonal meningioma who showed transient recent memory disturbance after surgery using this approach. Possible mechanisms of the patient's memory impairment are discussed.

2. Case report

A 57-year-old, right-handed woman had a history of depression, uterine myoma, and breast cancer. The patient complained of numbness of the lower extremities 2 months before admission, and underwent magnetic resonance imaging (MRI), which incidentally demonstrated a homogeneously enhanced mass at the trigonal region in the left lateral ventricle with a maximal diameter of 4 cm on T1-weighted images (Fig. 1, left and center). T2-weighted MR images demonstrated moderate edema around the mass (Fig. 1, right). Cerebral angiograms disclosed feeding arteries from the left anterior choroidal artery and the left medial and lateral posterior choroidal arteries, and venous pathways draining medially and laterally. The patient's neurologic examination was normal other than the complaints described above. Preoperative diagnosis was intraventricular trigonal meningioma.

* Corresponding author. Tel.: +81 86 235 7335; fax: +81 86 227 0191.
E-mail address: kojitoku@md.okayama-u.ac.jp (K. Tokunaga).

0090-3019/$ – see front matter
doi:10.1016/j.surneu.2005.06.036